

## Effects of Film Stress on the Chemical Mechanical Polishing Process

Wei-Tsu Tseng,<sup>a,\*</sup> Yiao-Hsien Wang,<sup>b</sup> and Jyh-Hwa Chin<sup>b</sup>

<sup>a</sup>Department of Materials Science and Engineering, National Cheng-Kung University, Tainan 701, Taiwan

<sup>b</sup>Department of Mechanical Engineering, National Chiao-Tung University, Hsinchu 300, Taiwan

A theoretical model is constructed to simulate the pressure distribution arising from wafer curvature (film stress) during chemical mechanical polishing (CMP), based on theories of elastic contact stress. Results from oxide CMP experiments suggest that the wafer curvature results in a nonuniform polish rate distribution across the wafer, in agreement with the simulation based on the model. This stress-dependent polish nonuniformity is attributed to the nonuniform pressure distribution across the wafer, induced by the wafer radius of curvature (film stress). Also, it was found that the magnitude of oxide film stress itself has little effect on removal rate. Oxides with tensile stress tend to have a weakened bond structure and enhanced chemical reactivity, both of which result in slightly higher removal rates. The reverse is true for oxides with compressive stress. Deviations from the model prediction may result from the stress induced by slurry flow, local variations in wafer shape and form, and pad surface properties.  
© 1999 The Electrochemical Society. S0013-4651(99)03-063-3. All rights reserved.

Manuscript submitted March 16, 1999; revised manuscript received July 1, 1999. This was in part Paper 1116 presented at the San Diego, California, Meeting the Society, May 5-7, 1998.

The proliferation of chemical mechanical polish (CMP) planarization in recent years has not been accompanied by an adequate level of knowledge of the fundamental mechanisms involved. Such a poor understanding inevitably leads to difficulties and often confusion when it comes to process control. Among the critical manufacturing issues, one of the challenges is to manage the within wafer nonuniformity (WIWNU). Mitigation of WIWNU through the adjustment of machine parameters, such as pad speed and down force, has been reported previously.<sup>1,2</sup> However, little has been revealed regarding the root cause of WIWNU, and a systematic methodology for controlling it does not yet exist. While it is generally agreed that pressure distribution and variation in relative velocity are the two main factors influencing WIWNU, how these two factors may vary in the presence of the rotating pad and carrier, the flowing slurry, and the wafer itself still remains obscure and deserves further investigation.

A further complication arises when the shape, *e.g.*, the curvature of the wafer is considered. Under the presence of down force and back-side pressure, the wafer curvature (characteristics of film stress) may induce uneven stress distribution along the direction normal to wafer, and irregular slurry flow on the plane of the wafer, both of which may contribute to WIWNU. Previous experimental results indicated that the magnitude of prepolish film stress (or wafer bow) affected both the removal rate and WIWNU. It was found in one study that the mean removal rate decreases while the WIWNU increases as the compressively stressed thermal oxide on one side of Si substrate (*i.e.*, convex wafer shape) was thinned down by the continuous polish process (*i.e.*, decreasing wafer bow).<sup>3</sup> Conversely, in another study,<sup>4</sup> both the removal rate and WIWNU were found to decrease with increasing prepolish wafer bow, from negative (concave, tensile stress) to positive (convex, compressive stress). Neither of the two studies above has given a proper physical model to account for the observed wafer curvature effects on the CMP process, although both speculated that the existence of the wafer bow makes it difficult to flatten the wafer when the carrier was pressed against it, giving rise to polish nonuniformity.

In this contribution, we examine the wafer curvature (film stress) effects on removal rate and WIWNU both theoretically and experimentally. A model based on Hertzian contact stress is proposed to simulate the wafer-scale pressure distribution, given carrier configuration, down force, back pressure, pad stiffness, and wafer curvature. In conjunction with a proper removal rate model, this calculated pressure profile can then be converted into theoretical WIWNU. Experiments with thermal and plasma-enhanced chemical vapor deposited (PECVD) oxides on the Si wafer with controlled stress level were performed to verify the validity of the proposed model.

The general effects of film stress upon removal rate and WIWNU are discussed.

### Model Construction

*Curvature-induced wafer-scale pressure distribution.*—There are many sources that can lead to wafer bow and deflection during integrated circuit (IC) manufacturing. In the current study, we consider only the deflection due to the existence of intrinsic and thermal film stresses. These stresses may be tensile (negative bow) or compressive (positive bow), depending on the deposition process and thermal history. First, the wafer is considered as a thin circular plate while the pad is regarded as a half space. The wafer/pad contact area is approximated as a bowl with radius  $a$  defined in Fig. 1. The applied down force exerts an axially symmetric uniform pressure profile onto the wafer. In order to simplify the case, the effect of slurry flow is neglected and the interaction between wafer and pad is assumed frictionless. In other words, this is the contact problem that obeys the conditions required by Hertzian contact theory.

Since the wafer is axially symmetric, all variables are constructed in the radial coordinate. In this case, the total pressure on the wafer surface can be expressed as the sum of separate pressure components

$$P_{\text{sum}} = P_{\text{uniform}} + \Delta P(P_{\text{contact}}) \quad [1]$$

where  $P_{\text{uniform}}$  is the wafer pressure arising from uniform down force,  $P_{\text{contact}}$  is the pressure intensity due to wafer contact, and  $P_{\text{sum}}$  is the sum of these pressures.

From Green's function for contact problem,<sup>5</sup> we can obtain the normal displacement  $u_y(x)$  at the point  $(x, 0)$  on the contact region as shown in Fig. 2

$$u_0(x) = -\frac{\kappa + 1}{4\pi G_w} \int_A p(\xi) \log|x - \xi| d\xi \quad [2]$$

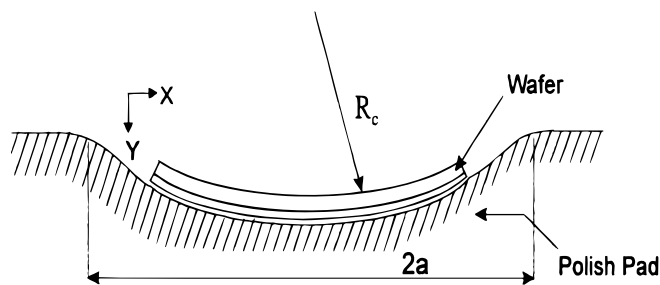


Figure 1. The perspective of contact between wafer and pad.

\* Electrochemical Society Active Member.

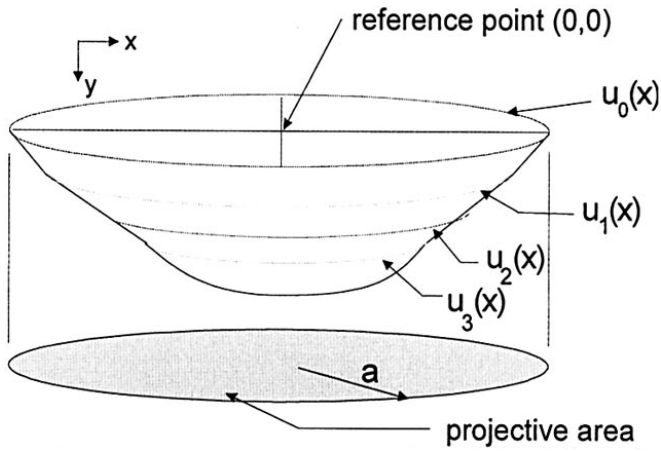


Figure 2. The perspective of function  $U_y(x)$  in wafer pad interface.

where  $x$  represents the position located on the contact region in horizontal direction,  $\kappa$  is plane stress ratio,  $u_0(x)$  is a function of  $x$  which describes the deflection at point  $(x, 0)$ ,  $u_y(x)$  is a function of  $x$  describing the deflection at point  $(x, y)$ .

Substituting Eq. 2 into Cauchy singular integral equation for unknown pressure  $p(\xi)$  yields the following expression

$$-\frac{du_0}{dx} = -\frac{(\kappa + 1)}{4\pi G_w} \int_{-a}^a \frac{p(\xi)d\xi}{x - \xi} \quad -a < x < a \quad [3]$$

The geometric relations of the contact area as shown in Fig. 3a and b require that

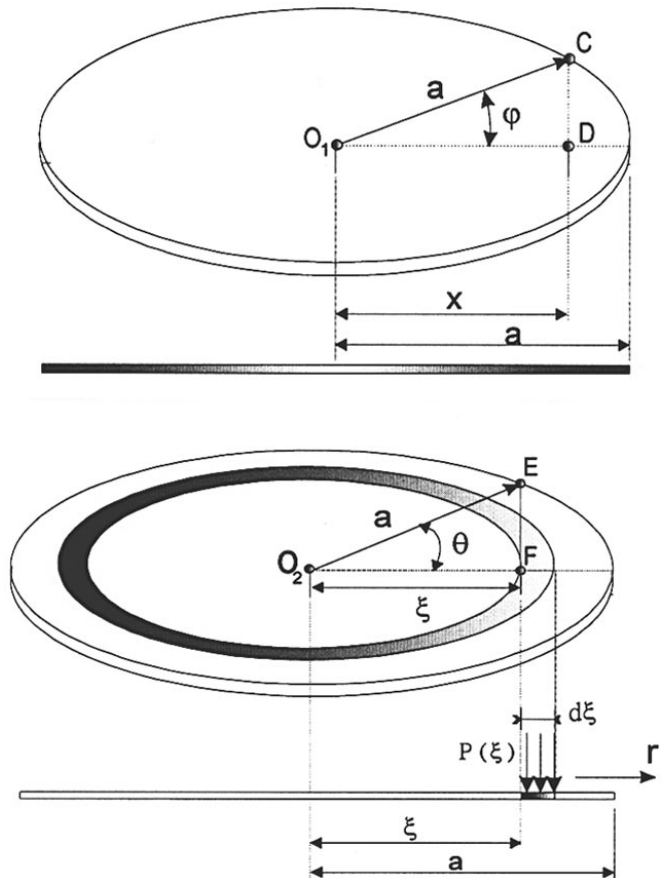


Figure 3. (a, top) A schematic showing point C on the contact area. (b, bottom) A schematic showing pressure  $P(\xi)$  on the contact area.

$$x = a \cos \varphi \quad \xi = a \cos \theta \quad [4]$$

where  $x$  is the horizontal distance between center and point  $C (\overline{O_1D})$ ,  $\varphi$  is the angle between  $\overline{O_1C}$  and  $\overline{O_1D}$ ,  $\xi$  is the horizontal distance between center and point  $E (\overline{O_2F})$  and  $\theta$  is the angle between  $(\overline{O_2E})$  and  $(\overline{O_2F})$ . Expanding both sides of Eq. 4 as a Fourier series, and substituting them into Eq. 3

$$\frac{1}{a \sin \varphi} \frac{du_0}{d\varphi} = -\frac{(\kappa + 1)}{4\pi G_w} \int_0^\pi \frac{p(\theta) \sin \theta d\theta}{(\cos \varphi - \cos \theta)} \quad 0 < \varphi < \pi \quad [5]$$

Using the formula proposed by Muskhelivili<sup>6</sup>

$$p(\theta) = \sum_0^\infty \frac{p_n \cos n\theta}{\sin \theta} \quad [6]$$

$$\frac{du_0}{d\varphi} = \sum_1^\infty u_n \sin n\varphi \quad [7]$$

one can find

$$\begin{aligned} \sum_{n=1}^\infty u_n \sin n\varphi &= \frac{(\kappa + 1)a \sin \varphi}{4\pi G_w} \sum_{n=1}^\infty \frac{\pi p_n \sin n\varphi}{\sin \varphi} \\ &= \frac{(\kappa + 1)a}{4G_w} \sum_{n=1}^\infty p_n \sin n\varphi \quad [8] \end{aligned}$$

and hence

$$p_n = \frac{4G_w u_n}{(\kappa + 1)a} \quad n > 1 \quad [9]$$

Also, the pressure, distribution  $p(\xi)$ , can be equated to the force  $F$  by the following

$$\begin{aligned} F &= -\int_A p(\xi)d\xi = \int_{-a}^a p(\xi)d\xi = \int_0^\pi p(\theta)a \sin \theta d\theta \\ &= -a \sum_{n=0}^\infty p_n \int_0^\pi \cos n\theta d\theta = \pi a p_0 \quad [10] \end{aligned}$$

Now, assume that the load  $F$  is sufficient to establish contact over the entire contact area, then the displacement of the half-plane must satisfy the condition

$$u_y(x) = -u_0(x) + C_1 x + C_0 \quad [11]$$

Let the curvature of the wafer be  $R_c$ , then the displacement is correlated with  $R_c$  and  $x$  by the following equations

$$\frac{d^2 u_0}{dx^2} = -\frac{1}{R_c} \quad [12]$$

$$u_0(x) = C_0 + C_1 \cdot x + \frac{x^2}{2R_c} = C_0 - \frac{a^2 \cos 2\varphi}{4R_c} - \frac{a^2}{4R_c} \quad [13]$$

Since the wafer is axially symmetric,  $u_0(x) = u_0(-x)$ , the results in  $C_1 = 0$ .

From Eq. 7 and 13, for a wafer with concave curvature, we have

$$u_2 = \frac{a^2}{2R_c} \quad [14]$$

$$p_2 = \frac{2G_w a}{R_c(\kappa + 1)} \quad [15]$$

so that the load is symmetrical to retain equilibrium and hence  $p_1 = 0$ . From Eq. 5, 10, and 15, the pressure can be expressed as a function of  $\theta$

$$p(\theta) = \left( -\frac{F}{\pi a} + \frac{2G_w a}{R_c(\kappa + 1)} \cos 2\theta \right) / \sin \theta \quad [16]$$

Equation 16 will be singular at  $\theta = 0$ ,  $\pi(x = \pm a)$  unless we choose an  $a$  such that

$$\frac{F}{\pi a} = \frac{2G_w a}{R_c(\kappa + 1)} \quad [17]$$

$$a = \sqrt{\frac{F(\kappa + 1)R_c}{2\pi\mu}} \quad [18]$$

For plane stress conditions

$$\begin{aligned} \kappa &= \frac{3 - \nu_w}{1 - \nu_w} \text{ and } \frac{2G_w}{(\kappa + 1)} = \frac{E_{com}}{4} \text{ where } \frac{1}{E_{com}} \\ &= \frac{1 - 2\nu_w}{E_w} + \frac{1 - 2\nu_p}{E_p} \end{aligned} \quad [19]$$

Substituting Eq. 18 and 19 into Eq. 16

$$p(\theta) = -\frac{F(1 - \cos 2\theta)}{\pi a \sin \theta} = -\frac{2F \sin \theta}{\pi a} \quad [20]$$

$$p(x) = -\frac{2F\sqrt{a^2 - x^2}}{\pi a^2} \quad [21]$$

where  $F$  is line load on the wafer. Since  $F = 2\pi a \tilde{P}$ , where  $\tilde{P}$  is the pressure from down force and  $r \cong x$  when  $R_c \gg r$ , Eq. 20 can be re-expressed as

$$P_{contact} = p(r) = -\frac{4\tilde{P} \cdot R_w}{a} \sqrt{1 - \left(\frac{r}{a}\right)^2} \text{ and } p(0) = \frac{-4\tilde{P} \cdot R_w}{a} \quad [22]$$

In a similar fashion, we can solve for the case of wafer with convex curvature

$$\frac{d^2 u_0}{dx^2} = \frac{1}{R_c} \quad [23]$$

$$p(\theta) = -\frac{F(1 + \cos 2\theta)}{\pi a \sin \theta} = -\frac{2F}{\pi a} \left( \sin \theta - \frac{1}{\sin \theta} - 1 \right) \quad [24]$$

and

$$P_{contact} = p(r) = \frac{2\tilde{P}R_w}{a} \left( \sqrt{\frac{a^2 - R^2}{a^2}} - \sqrt{\frac{a^2}{a^2 - r^2}} - 1 \right) \quad [25]$$

The back pressure  $P_{back-pressure}$  is applied onto the wafer numerically, the pressure intensity due to back pressure is derived from the force equilibrium method in our previous publication.<sup>7</sup> The overall pressure  $P_{sum}$  is the summation of the above, *i.e.*

$$P_{sum} = P_{uniform} + P_{contact} + P_{back\ pressure} \quad [26]$$

*Correlation between wafer curvature and film stress.*—Thin film deposition process and postdeposition thermal treatments induce stresses in the film as manifested by the change in wafer curvature. In an ideal case, the film stress is obtained by the Stoney equation<sup>8</sup>

$$\sigma = \frac{E_w}{1 - \nu_w} \frac{h_w^2}{6R_c h_f} \quad [27]$$

where  $E_w/1 - \nu_w$  is biaxial modulus of the substrate (silicon wafer),  $h_w$  is substrate thickness,  $h_f$  is film thickness,  $R_c$  is radius of curvature, and  $\sigma$  is the film stress. To calculate the change in film stress, the following equation is used

$$\sigma = \frac{E_w}{6h_f} \frac{h_w^2}{1 - \nu_w} \left( \frac{1}{R_{c1}} - \frac{1}{R_{c2}} \right) \quad [28]$$

where  $R_{c1}$  is the curvature before film deposition, and  $R_{c2}$  is the curvature after the process. Assuming the wafer is bent symmetrically, the following relationship can be constructed according to the schematic in Fig. 4

$$2R_w = R_c \theta_{AB} \quad [29]$$

$$\frac{D_{AB}}{2} = R_c \cdot \sin\left(\frac{\theta_{AB}}{2}\right) \quad [30]$$

where  $D_{AB}$  is the distance between point A and point B,  $\theta_{AB}$  is the angle between  $OA$  and  $OB$ , and  $h_g$  is the gap distance between wafer and pad.

Since  $\theta_{AB}$  is small, Eq. 30 can be reduced to

$$\frac{D_{AB}}{2} = R_c \frac{\theta_{AB}}{2} \quad [31]$$

substituting Eq. 31 into Eq. 29 yields

$$D_{AB} = 2R_w \quad [32]$$

the maximum deflection of wafer  $h_g$  at center is given by

$$h_g = R_c - R_c \cos \frac{\theta_{AB}}{2} \quad [33]$$

also, from geometry

$$\sin \frac{\theta_{AB}}{2} = \frac{D_{AB}}{2R_c} \quad [34]$$

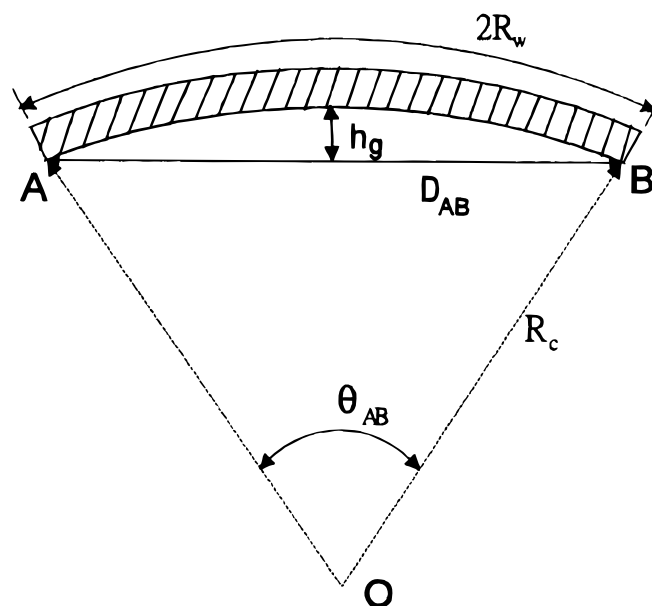


**Figure 4.** The geometrical relationship of wafer bow. In this case, the wafer is said to have a downward radius of curvature, manifesting the existence of compressive stress.

then, substitution of Eq. 34 into Eq. 33 results in the expression for the maximum wafer deflection  $h_g$

$$h_g = R_c - R_c \left[ 1 - \left( \frac{D_{AB}}{2R_c} \right)^2 \right]^{\frac{1}{2}} \rightarrow (h_g - R_c)^2 = R_c^2 - \frac{D_{AB}^2}{4} \quad [35]$$

since  $R_c \gg h_g$ , Eq. 35 can be rewritten as

$$h_g \equiv \frac{D_{AB}^2}{8R_c} \quad [36]$$

Additionally, since  $D_{AB}$  is small compared with  $R_c$ ,  $D_{ab}$  can be considered as a constant and then

$$h_g \propto \frac{1}{R_c} \quad [37]$$

again from Eq. 34

$$\sin\left(\frac{\theta_{AB}}{2}\right) = \frac{D_{AB}}{2R_c} \rightarrow \theta_{AB} \equiv \frac{D_{AB}}{R_c} \quad [38]$$

So, with a given film stress and  $\theta_{AB}$  (e.g., from standard laser scanning technique), the deflection of wafer  $D_{AB}$  and the gap distance  $h_g$  can be determined, and the wafer-scale pressure distribution can be calculated from Eq. 24, 25, and 26.

The pressure profiles calculated based on the model above can be fitted into appropriate polish rate models to determine the theoretical and removal rate and WIWNU. In this study, both Preston's equation ( $R.R. = K_p PV$ ) and Tseng's model ( $R.R. = MP^{5/6} v^{1/2}$ , where  $M$  is a weighing parameter)<sup>9</sup> are used to determine the theoretical removal rates. The latter has been demonstrated experimentally to be a more accurate removal rate model for oxide CMP<sup>10</sup> and is included here for comparison with the Preston equation.

### Experimental

Thermal oxides (wet oxides) and PECVD tetraethoxysilane/ozone (TEOS/O<sub>3</sub>) oxides were grown/deposited on 150 mm wafers up to a thickness of ~1200 nm. As defined in Fig. 4, stresses in oxide films are carefully tuned to be tensile (upward curvature) or compressive (downward curvature), by varying the deposition conditions. CMP experiments were conducted on an IPEC 472 polish system with a "K-groove" pad, R-200 carrier film, and SC-112 slurry. The down force and back-side pressure for thermal oxide polish were fixed at 7 and 0 psi, respectively; while those for TEOS/O<sub>3</sub> oxides were varied. The platen and carrier rotations are set at 20 and 42 rpm, respectively, for thermal oxides; and 30 and 28 rpm, respectively, for TEOS/O<sub>3</sub> oxides. *Ex situ* pad dressing was performed at the end of each polish run. These oxide wafers were polished at 1 min intervals up to 7 min. At the end of each min, the wafer curvature and stress were measured using the standard laser beam wafer deflection technique. Removal rate and WIWNU (1- $\sigma$ ) were measured and calculated at 49 points across each wafer, considering a 4 mm edge exclusion.

### Results and Discussion

**Calculated wafer level pressure distribution.**—The pressure distribution across a wafer under a given down force can be calculated from principles of Hertzian contact stress.<sup>5</sup> Under a down force of 6 psi, the pressure distribution across a 150 mm wafer in contact with an IC1000/Suba IV composite pad on an IPEC 472 polisher is nonuniform, with distant edge high characteristics as shown in Fig. 5. In fact, such an across-wafer pressure distribution also correlates well with the removal rate profile along the wafer diameter, as observed in our previous study.<sup>7</sup> The pressure at wafer center is merely 5.5 psi, while that at the edge may be as high as 12 psi. When the wafer curvature (e.g., downward curvature) is considered, the pressure distribution is modified, due to the nonuniform elastic response from the

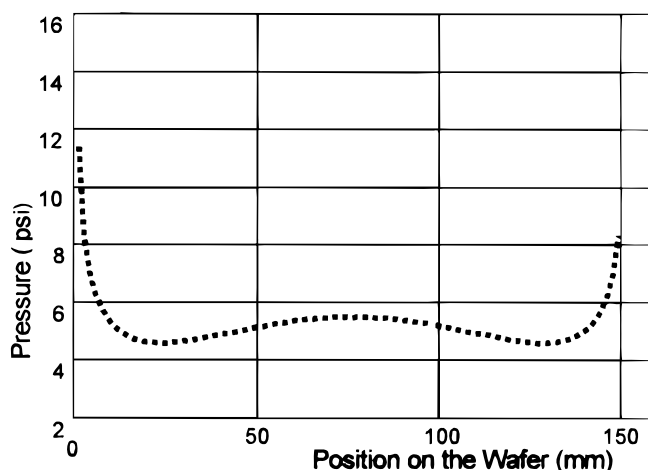


**Figure 5.** Wafer pressure distribution on a flat 150 mm wafer under a down force of 6 psi and back pressure of 0 psi. The polisher and pad used are IPEC 472 and K grooved, respectively.

curved wafer to the applied down force. This can be seen clearly from Fig. 6, which is calculated based on the model proposed in this study. The wafer with a downward curvature is held upside down by the carrier, and a down force of 7 psi is exerted along the center axis of the wafer. The actual pressure experienced by the wafer at its center is elevated due to the wafer curvature effect.

To provide a better view for this curvature effect, the pressure profiles for wafers with upward and downward curvature are calculated for different radius of curvature, and the results are exhibited in Fig. 7 and 8, respectively. In both cases, the pressures at the wafer edge are larger, in agreement with previous simulation studies.<sup>7,11</sup> For wafers with upward curvature (i.e., tensile stress), the pressure is increased across the entire wafer compared with "flat wafers," such a curvature-induced pressure increase is more pronounced for wafers with larger radius of curvature (lower tensile stress). The situation is slightly different for wafers with downward curvature (compressive stress). In this case, the pressure is also increased and a larger radius of curvature (lower stress) also induces a greater effect. However, the difference in pressure reduces gradually from wafer center to wafer edge, and diminishes eventually at a certain point close to the edge, after which the trend reverses and a shorter downward radius of curvature (larger compressive stress) brings about a greater pressure increase. The variation in pressure distribution described above is the root of polish nonuniformity as is discussed later in this paper.

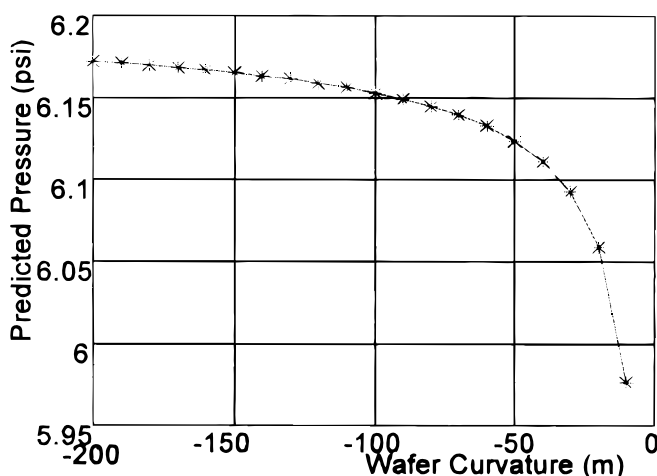


**Figure 6.** Predicted (calculated) pressure at wafer center in the presence of downward curvature. Down force = 7 psi; back-side pressure = 0 psi.



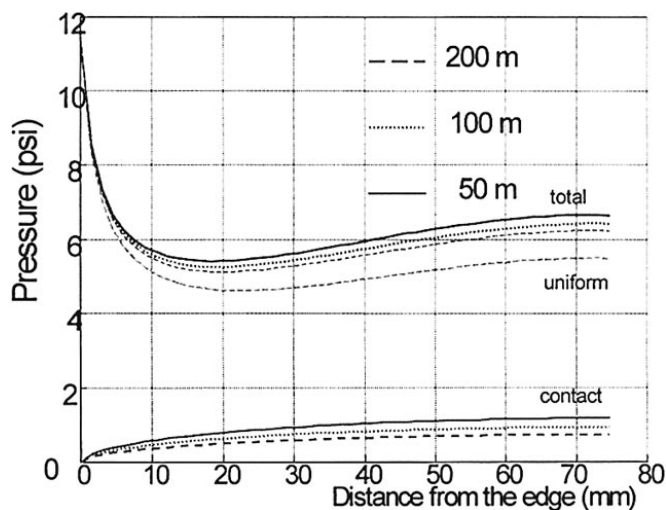


**Figure 7.** Across-wafer pressure profile for three different upward radii of curvature. (Down force = 6 psi; contact = contact stress.)

*Correlation between film stress and removal rate.*—Mean removal rates are plotted against upward and downward wafer curvatures of oxide films in Fig. 9 and 10, respectively. The corresponding film stress is also shown for comparison. For each curvature, three wafers were polished and their removal rates were averaged to give a data point on the figures. As shown, for wafers with an upward curvature (tensile stress), the CMP removal rates increase slightly with decreasing radius of curvature (increasing tensile stress). The reverse is true for wafers with a downward radius of curvature (compressive stresses).

Cross comparisons between Fig. 7 through 10 suggest that, for oxides with tensile stresses, a smaller film stress (larger radius of curvature) associated with a greater pressure gives rise to a lower (though only marginally) removal rate. Conversely, for wafers with compressive stresses, a smaller stress and thus a greater pressure would result in a higher removal rate. The two behaviors above seem contradictory to one another, since, according to the removal rate models (e.g., Preston's equation), a greater pressure corresponds to an accelerated wearing rate and hence a higher removal rate.

Haque *et al.* reported that the existence of a tensile stress component in the oxide network would make the bonds more reactive and result in a more open structure of the  $(\text{SiO}_2)_n^{-4}$  tetrahedral net-

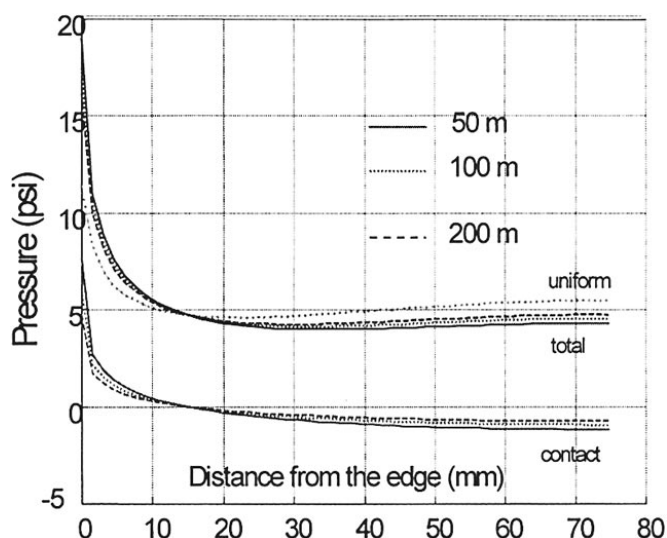


**Figure 8.** Across-wafer pressure profile for three different downward radii of curvature. (Down force = 6 psi; back-side pressure = 0 psi.)

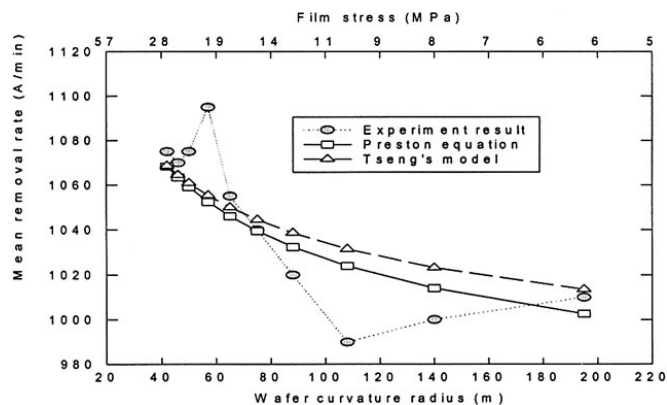


**Figure 9.** Mean removal rates vs. wafer upward radius of curvature for thermal oxide films. The corresponding compressive stress is also included for comparison.

work in the oxide.<sup>12</sup> As a consequence, the oxide structure would become more susceptible to the chemical attack by alkaline slurry, leading to a higher removal rate. From another perspective, Nogami and Tomozawa pointed out that the water diffusion rate in silica is a function of local stress.<sup>13</sup> A local tensile stress in the film leads to an enhanced diffusion coefficient of water of  $\text{H}^+$  in silica. As a consequence, the presence of a higher tensile stress in the oxide film would induce a high CMP removal rate through accelerated water/slurry diffusion and the stronger reactivity with the alkaline agent in the slurry. Therefore, the observed removal rate variation can be explained by this stress-assisted chemical erosion effect. For oxides in tension, a lower tensile stress translates to a more moderate stress-assisted chemical effect and hence a lower CMP removal rate. Similarly, for oxides in compression, a lower stress would give rise to lower resistance to wearing and chemical erosion, and hence a slower removal rate.

Several previous studies indicated that the CMP removal rate of oxides and nitrides is also a strong function of their bonding configuration, which is manifested by density and refractive index (RI) in the thin films.<sup>14,15</sup> In the present study, the measured RI for the thermal oxides falls between 1.455 and 1.459, suggesting that the oxides are nearly stoichiometric ( $\text{IR} \sim 1.46$ ) having virtually the same density. Therefore, we ruled out the effects of density change as the possible cause for the removal rate variation in Fig. 7 to 10.

The fluctuation of mean removal rate in Fig. 9 and 10 may come from multiple sources. First, the mean removal rate is, by its nature, a statistical value averaged over the entire wafer. Nonuniform slurry flow and pad surface condition may have led to the variation of removal rate. In addition, the model proposed in this study is derived

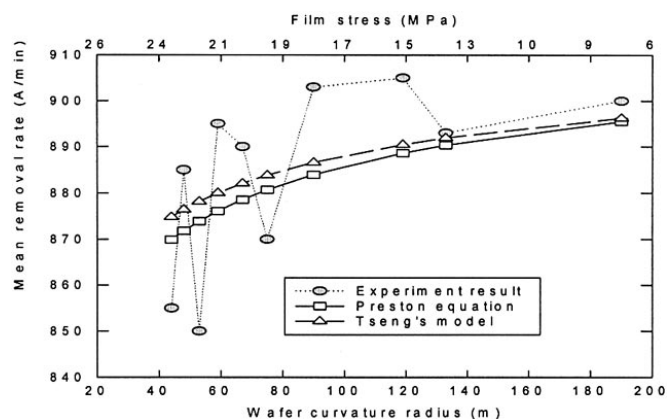


**Figure 10.** Mean removal rate vs. wafer downward radius of curvature for thermal oxide films. The corresponding compressive stress is also included for comparison.

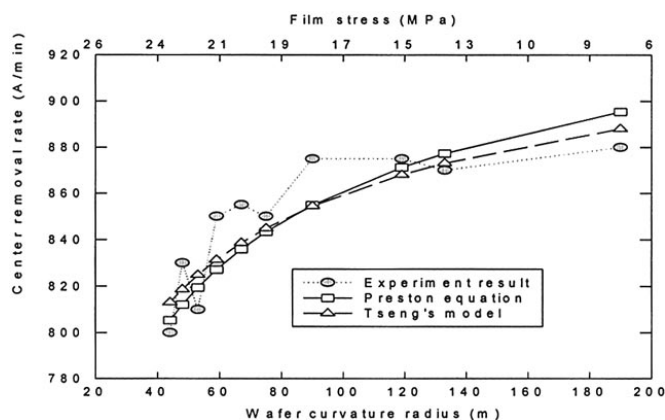


**Figure 11.** Wafer center removal rate vs. downward radius of curvature and compressive stress for thermal oxide films.

based on the assumption that the wafer is axially symmetric, meaning that the curvature (film stress) and wafer shape is uniform. Any deviation (as is usually the case) from this simplification would result in removal rate fluctuation and discrepancy between model prediction and experimental data. Adding to the above complexity is the fact that, in reality, the thin films being polished are deposited over patterned line or hole features distributed across the entire wafer. This would lead to local variations in stress and wafer form, and introduce more fluctuation and scattering in the polish data.

Overall, the results above seem to indicate that the stress-induced bond weakening/strengthening mechanism plays a certain role in the removal process to the extent that it may dominate over the down pressure in determining the removal rate. Still more work is needed to verify this point.

*Stress-induced pressure distribution and polish nonuniformity.*—To further clarify the curvature effect, the evolution of CMP removal rates with the changing wafer curvature were monitored at specific locations on a wafer. Figures 11 and 12 show the center and edge removal rates, respectively, for films with compressive stresses (downward curvature). As polish proceeds, compressive stress (radius of curvature) in the film is relieved (increased), the center removal rate increases from 810 Å/min at  $-24$  MPa (radius of curvature = 46 m) to 876 Å/min at  $-15$  MPa (radius of curvature = 125 m). Meanwhile, the edge removal rate (measured at  $\sim 5$  mm away from wafer periphery) decreases from 1003 to 943 Å/min correspondingly. This would rise to a reduced WIWNU since the difference in polish rate diminishes gradually as polishing progresses. The

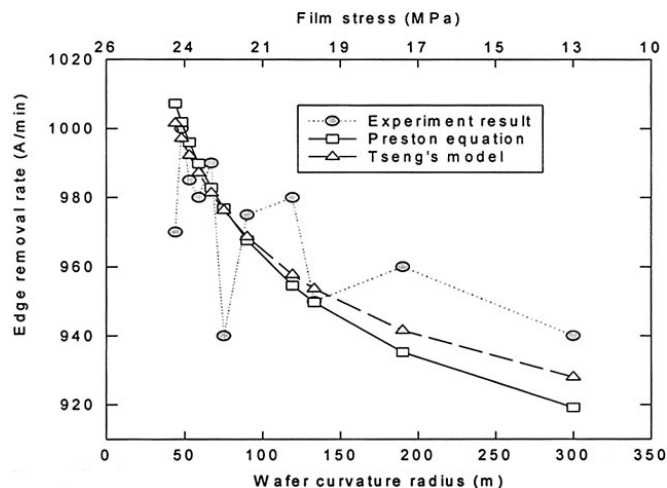


**Figure 12.** Wafer edge removal rate vs. downward radius of curvature for thermal oxide films.

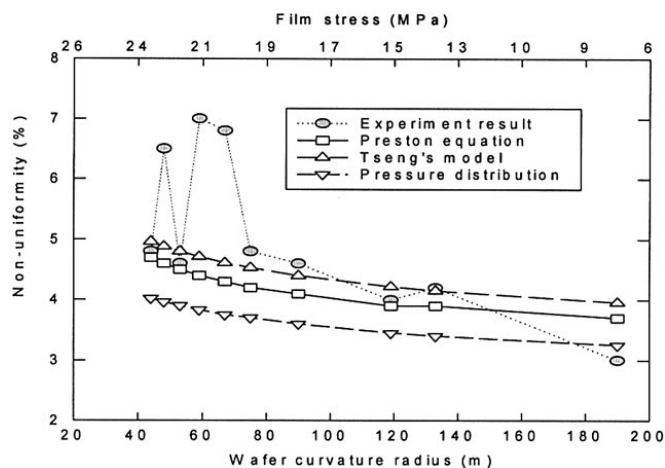


**Figure 13.** Pressure and polish nonuniformity (WIWNU) as a function of wafer downward radius of curvature and compressive stress.

different trends in removal rate at the wafer center and edge are the direct consequence of the curvature-induced pressure profile as shown in Fig. 8. The pressure and WIWNU are expressed in terms of downward wafer radius of curvature in Fig. 13. As can be seen, both the pressure and polish nonuniformity decrease as compressive stress in the film is relieved. In other words, a “flatter” wafer (*i.e.*, smaller stress and larger radius of curvature) would induce a more uniform distribution and thus more uniform material removal during CMP. The correlation between calculated pressure nonuniformity and the experimental WIWNU is distinct. The close agreement between the experimental polish rate and WIWNU and those predicted by the model proposed demonstrates the validity of the model. As polish progresses, the relief in-plane compressive stress due to the thinning of oxide film induces a more uniform distribution of the out-of-plane down pressure across the wafer, leading to a reduced WIWNU. For wafers with upward radius of curvature (tensile stress), the curvature-induced pressure increase should be uniform across the entire wafer as found in Fig. 7. As shown in Fig. 14, and 15, both center and edge removal rates decrease with increasing wafer radius of curvature, in agreement with the prediction. In this case, the curvature effect does not help significantly in reducing the polish nonuniformity since the removal rates at edge and center were increasing concurrently. The WIWNU after the first minute of polish (radius of curvature = 48 m) is 5.64% (measured) and 4.95 (calculated); while the WIWNU after the last minute of polish (radius of curvature = 190 m) is 5.38% (measured) and 4.55% (calculated).

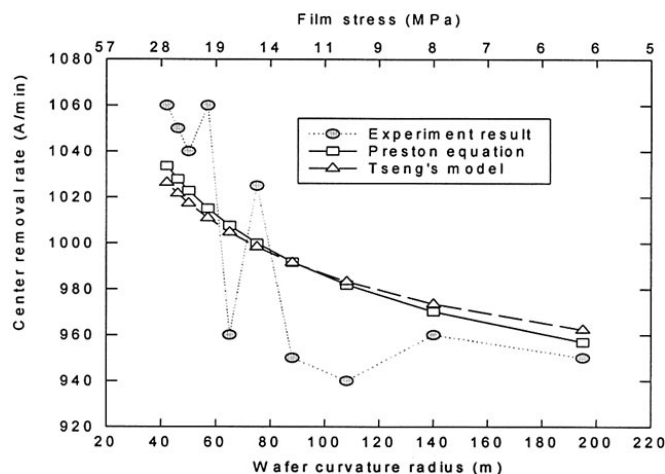


**Figure 14.** Wafer center removal rate vs. upward radius of curvature for thermal oxide films.

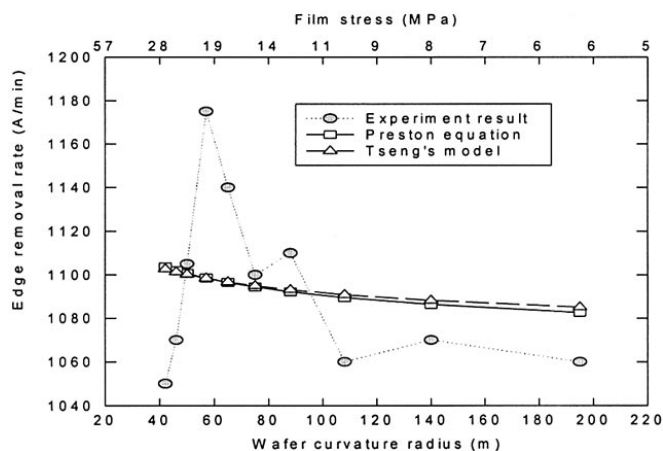


**Figure 15.** Wafer edge removal rate vs. upward radius of curvature for thermal oxide films.

Also noted from the figures above (e.g., Fig. 13) is that the theoretical WIWNU based on the Tseng's model (standard deviation,  $\sigma = 145$ ) is in closer agreement with the experimental results than the one based on the Preston equation ( $\sigma = 2.76$ ). This may imply that Tseng's model is more feasible in predicting the CMP removal rate and its nonuniformity as a function of pressure and velocity. Similar results were also found in our previous studies.<sup>9,10</sup>

As a further illustration of the model, the effect of back-side pressure is also investigated. In this case, PE-TEOS oxides with an initial downward radius of curvature (25 m, stress = -53 MPa) were polished, and the variation of a 49 point mean removal rate was calculated and experimentally measured. The results in Fig. 16 indicate an increasing trend of removal rate with decreasing wafer radius of curvature (compressive stress), similar to the result in Fig. 11 for thermal oxide. When the down force is raised to 11 psi and a back-side pressure of 4 psi is applied, the pressure profile is raised and the removal rates are enhanced. The match between the experiments and theoretical prediction is excellent in both cases.

*General remarks.*—Several points can be drawn regarding the stress effects on oxide CMP process based on the results gained in this study. The film stress itself does not contribute significantly to the reduction (compressive stress) or enhancement (tensile stress) of the CMP removal rate. It does, however, induce a redistribution of pressure across the wafer, causing a variation in the mean removal rate and WIWNU. Since the wafer radius of curvature increases as polish progresses, the horizontal axes in Fig. 9 through 15 can be taken as the polish time so that they actually represent the variations of removal rate or nonuniformity with polish time. Such a phenomenon is frequently encountered in the CMP process, and can now be attributed to the stress (curvature) effect. In addition, the so-called substrate effect,<sup>16,17</sup> in which the removal rate was found to increase or decrease depending on the substrate material beneath the layer being polished, may actually arise, at least partially, from the curvature effect described in the present study.

For metal CMP, the stress effects may become even more complicated. Due to their high thermal expansion of coefficient relative to the dielectric substrate, most of the metals, whether W, Al, or Cu, exhibit a tensile stress after deposition. The bond weakening/strengthening mechanism due to stress may also be applicable to metal thin films. However, its net influence on the removal rate may be diluted since an additional plastic deformation energy should be overcome before the metal atom clusters can be broken and polished off. In addition, other attributes, such as grain size<sup>18</sup> and texture,<sup>19</sup> may overwhelm this stress effect so that it would be difficult to evaluate the direct impact of stress on the metal CMP removal rate. Finally, the existence of tensile stress in metal films implies that the WIWNU may not decrease with time due to the wafer curvature effect, as in the

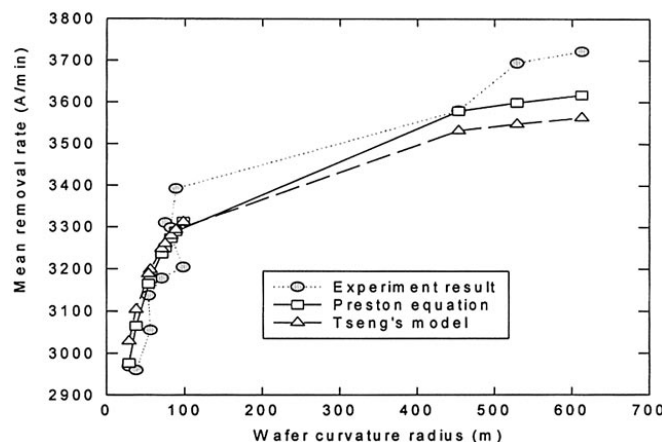
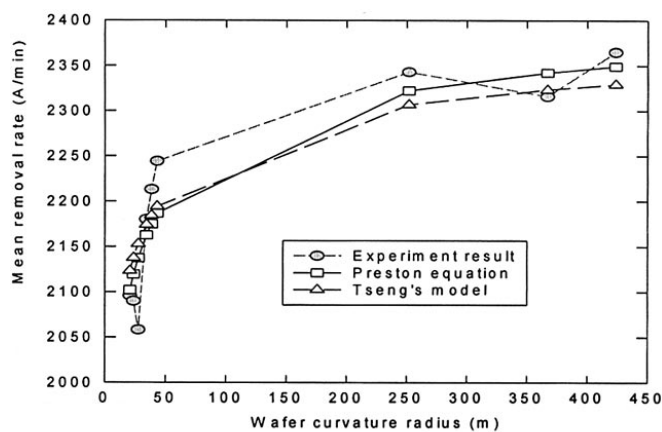


**Figure 16.** Experimental and theoretical (based on the Preston equation and Tseng's model) CMP removal rates for PE-TEOS oxide films with an initial downward radius of curvature (=25 m). [(a, top) Down force = 7 psi; back-side pressure = 0 psi. (b, bottom) Down force = 11 psi; back-side pressure = 4 psi.]

case of oxide CMP. Further experimental work is required to verify the speculation above.

Influences from other physical events, such as fluid flow and pad surface feature, in the presence of wafer curvature should be considered in the modeling in order to gain further insight into the origins of polish nonuniformity. Future work for this study would include the variations of down force and back-side pressure in the simulation and experiments for a more thorough control over the nonuniformity issue.

## Conclusion

A model based on Hertzian contact theory is proposed to calculate the pressure along the pad/wafer interface under a given down force, back-side pressure, and backing film. The resulting pressure profile, removal rate, and nonuniformity across the wafer can be determined theoretically. The film stress itself does not bring about a significant change in removal rate. However, it induces a redistribution of pressure profile that modifies WIWNU. Given an "edge high" polish characteristic, the WIWNU decreases with the decreasing compressive stress (increasing downward radius of curvature) in the film, as polish proceeds. For wafer with tensile stress (upward radius of curvature), the removal rate increases slightly in the presence of stress, and the WIWNU does not change significantly with time due to this curvature-induced pressure effect. Parameters such as slurry flow behavior, local variation in wafer form, and pad surface properties may interact with the wafer curvature effects and cause deviations in removal rates and WIWNU predicted by the model.

### Acknowledgments

The authors are grateful to Dr. Chi-Fa Lin of Winbond Electronics Corporation (TD, FAB IV), Taiwan, for his kind assistance in performing the polishing experiments and other equipment support. This work is supported by the National Science Council of Taiwan under contract number NSC 88-2216-E-006-042, and the Chung-Shan Institute of Science and Technology.

National Cheng-Kung University assisted in meeting the publication costs of this article.

### References

1. I. Ali, S. R. Roy, and G. Shinn, *Solid State Technol.*, **37-10**, 63 (1994).
2. A. Modak, P. Monteith, and N. Parikh, in *1997 CMP-MIC Proceedings*, p. 169, IMIC, Tampa, FL (1997).
3. C.-H. Liu, M.S. Thesis, Institute of Electronics, Chiao-Tung University, Taiwan (1995).
4. Y. Zhang, P. Parikh, P. Golubtsov, B. Stephenson, M. Bonsaver, J. Lee, and M. Hoffman, in *Chemical-Mechanical Planarization for IC Device Manufacturing*, I. Ali and S. Raghavan, Editors, PV 96-22, p. 91, The Electrochemical Society Proceedings Series, Pennington, NJ (1997).
5. H. Hertz, *Ann. Phys. Chem.*, p. 492 (1882) in German.
6. N. I. Mushelishvili, *Some Basic Problems of the Mathematical Theory of Elasticity*, translated from Russian by J. R. M. Radok, P. Noordhoff, Ltd., Groningen, The Netherlands (1963).
7. W.-T. Tseng, L.-C. Kang, W.-C. Pan, J.-H. Chin, and P.-Y. Chen, in *1998 CMP-MIC Proceedings*, p. 87, IMIC, Tampa, FL (1998).
8. G. C. Stoney, *Proc. R. Soc. London, Ser. A*, **82**, 172 (1909).
9. W.-T. Tseng and Y.-L. Wang, *J. Electrochem. Soc.*, **144**, L15 (1997).
10. W.-T. Tseng, L.-C. Kang, and J.-H. Chin, *J. Electrochem. Soc.*, **146**, 1952 (1999).
11. A. R. Baker, in *Chemical-Mechanical Planarization for IC Device Manufacturing*, I. Ali and S. Raghavan, Editor, PV 96-22, p. 228, The Electrochemical Society Proceedings Series, Pennington, NJ (1997).
12. M. S. Haque, H. A. Naseem, and W. D. Brown, *J. Appl. Phys.*, **82**, 2922 (1997).
13. M. Nogami and M. Tomozawa, *J. Am. Ceram. Soc.*, **67**, 151 (1984).
14. C.-W. Liu, B.-T. Dai, and C.-F. Yeh, *J. Electrochem. Soc.*, **142**, 3098 (1995).
15. C.-F. Lin, W.-T. Tseng, M.-S. Feng, and Y.-L. Wang, *Thin Solid Films*, **347**, 24 (1999).
16. Y.-L. Wang, C. Liu, M.-S. Feng, J. Dun, and K.-S. Chou, *Thin Solid Films*, **308-309**, 543 (1997).
17. C. G. Kallingal, M. Tomozawa, and S. P. Murarka, *J. Electrochem. Soc.*, **145**, 1790 (1998).
18. J. Wu, M.S. Thesis, Institute of Materials Science and Engineering, National Tsing-Hua University, Taiwan (1996).
19. L. Vanasupa, D. Pinck, Y.-C. Joo, T. Nogami, S. Pramanic, S. Lopatin, and K. Yang, *Electrochem. Solid-State Lett.*, **2**, 275 (1999).